Probing the fields in an ultracold plasma by microwave spectroscopy

Hyunwook Park, Raheel Ali,* and T. F. Gallagher
Department of Physics, University of Virginia, Charlottesville, Virginia 22904-0714, USA
(Received 1 July 2010; published 26 August 2010)

By observing the Stark shift of the Rb $42s_{1/2}$-$42p_{1/2}$ microwave transition we have measured the electric fields in an ultracold plasma formed by photoionizing Rb atoms in a magneto-optical trap. Using this approach and a model of the electron charge distribution we have been able to measure both the microscopic fields due to nearest-neighbor ions and the macroscopic fields due to the charge imbalance in the plasma.

DOI: 10.1103/PhysRevA.82.023421 PACS number(s): 32.60.+i, 32.80.Ee, 32.80.Fb

I. INTRODUCTION

Since their introduction a decade ago, ultracold neutral plasmas produced from atoms in a magneto-optical trap (MOT) have generated a great deal of interest [1–3]. There are two appealing features of these plasmas. First, they have well-defined initial conditions, and second, they offer the prospect of strongly coupled plasmas [2,3], perhaps leading to crystallization, as observed in single-component cold-ion plasmas [4,5]. Although the plasmas are initially cold, several mechanisms heat the plasma. The random spacing of the MOT atoms leads to heating of the ions when the atoms are photoionized [6,7] and the plasma electrons are heated by three-body recombination of the electrons, followed by superelastic electron-Rydberg atom collisions [8–12]. An aspect of these plasmas which has not been measured is the electric field. Plasmas have, in general, two kinds of electric fields, microscopic and macroscopic fields. The microscopic fields come from the ions in the plasma, which are so slowly moving that they produce quasistatic fields [13,14]. For any atoms but one at the edge of the plasma, the fields from distant ions average to zero, and it is the field of the nearest-neighbor ion which is most important. Accordingly we approximate the microscopic field by the inverse square of the distance to the nearest ion, leading to a $\rho_I^{2/3}$ dependence. We ignore the electrons since they move rapidly and all do not in any way resemble a quasistatic field. The macroscopic fields are due to, for example, the applied field in a discharge or the charge imbalance in a nonneutral plasma. An example of the latter occurs in an ultracold plasma formed by photoionizing the cold atoms held in a MOT [1]. A fraction of the photoelectrons leave and the remainder are trapped by the excess positive charge of the cold, approximately motionless ions. The higher the energy of the photoelectrons the larger the excess positive charge required to trap the electrons [1–3]. If the photoelectrons initially have very low energy the resulting plasma is very nearly a neutral plasma, with as little as a 1% charge imbalance.

A classic method of measuring the fields in low-density plasmas is measuring the Stark shift and broadening of atomic transitions [15]. Laser spectroscopy of Rydberg states has been used to measure the fields in both the cathode fall and positive column of low-pressure gas discharges [16,17], and fields as low as 10 V/cm have been measured with this approach. In all the discharge measurements the fields were macroscopic fields. The microscopic fields, expected to be 0.1 V/cm in their case [16], were too small to measure with the available 10 GHz laser resolution. While the resolution was limited by the laser linewidths, due to the Doppler broadening of the optical transitions the resolution and field sensitivity cannot be improved by much in any case. Recently the fields in highly nonneutral ultracold plasmas, termed Coulomb clusters, of Rb have been measured by a similar technique [18]. Rb $5p$ atoms in a MOT were photoionized with a 355 nm laser pulse, creating photoelectrons with approximately 1 eV of energy. Most of the electrons leave, and the macroscopic field due to the net positive charge is probed by a delayed second laser to observe the Stark broadening of the excitation spectrum from the Rb $5p$ state to the Rydberg states. Fields as low as 10 V/cm were observed, due to the macroscopic field from the excess positive charge. The microscopic fields were too small to observe with the 10 GHz laser resolution, although in this case the Doppler broadening does not present an inherent problem.

Here we report the measurements of the fields in an ultracold Rb plasma using a method similar to that employed by Feldbaum *et al.* [18], but with two important differences. First, we use a dye laser to photoionize the Rb $5p$ atoms, allowing us to produce photoelectrons with energies from 1 to 143 cm^{-1}, corresponding to temperatures of 1 to 206 K, allowing the production of more nearly neutral plasmas. Second, we probe the fields after the plasma is created by exciting Rb $42s$ atoms with a second laser and driving the $42s$ to $42p$ microwave transition and observing its Stark shift. The linewidth of the microwave transition is 5 MHz, and the Stark shift of the $42s$ to $42p$ transition is 33 MHz/$(V/cm)^2$. We can observe frequency shifts in the line which are 10% of its width, enabling us to detect fields as low as 0.1 V/cm, which enables us to observe both the microscopic and macroscopic fields.

In the sections which follow we describe the experimental approach, present our observations, and extract the fields by applying a simple model to these observations.

II. EXPERIMENTAL APPROACH

Many details of the apparatus can be found elsewhere, so we here outline only the essential features [19]. As shown in Fig. 1, cold Rb atoms are held in a vapor-loaded MOT, at the center of a four rod structure used to apply static and pulsed electric fields, the latter for field ionization and charged

*Permanent address: Department of Physics, Quaid-i-Azam University, Islamabad, Pakistan 45320.

 ©2010 The American Physical Society

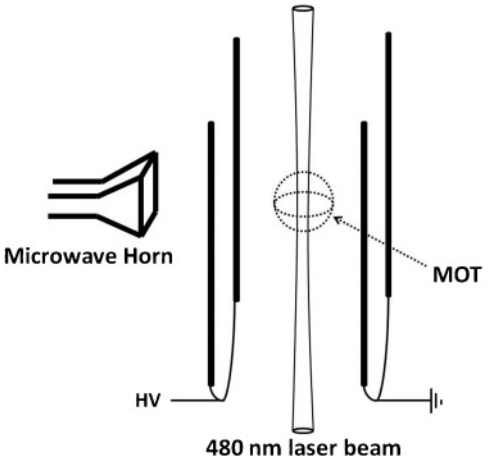

FIG. 1. Schematic diagram of the apparatus. The six 780 nm MOT beams and the vacuum envelope are not shown, and the microwave horn is outside the vacuum envelope. The 480 nm laser beams produce cylindrical volumes of plasmas and Rydberg atoms.

particle collection. The cold atom cloud has a diameter of approximately 1 mm and a density of up to $\sim 10^{10}$ cm^{-3}. The trap lasers provide a steady-state population in the $5p_{3/2}$ state, and we excite atoms from this state with two 8 ns ~480 nm laser pulses at a repetition rate of 15 Hz. The timing of the experiment is shown in Fig. 2. The first laser pulse is a dye laser pulse which excites the $5p_{3/2}$ atoms to energies from 1 to 143 cm^{-1} above the ionization limit. The excess energy above the ionization limit determines the electron energy and temperature in the plasma. The second pulse, at a time t from 10 ns to 20 μs later, excites atoms from the $5p_{3/2}$ state to the $42s$ state. The spatially overlapped 480 nm beams are focused to diameters of 160 μm and pass vertically through the center of the MOT, as shown in Fig. 1, producing a cylindrical volume of both plasmas and $42s$ Rydberg atoms. The second laser pulse, to excite atoms to the $42s$ state, is from a frequency doubled 960 nm diode laser, which produces

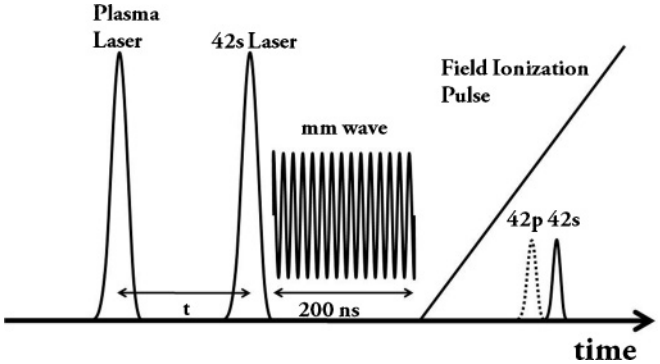

FIG. 2. Timing diagram for the experiment. The first, plasma laser pulse produces the ultracold plasma. The second, $42s$ laser pulse, which is delayed by time t, produces the probe $42s$ atoms. The microwave pulse immediately after the second laser pulse is used to drive the $42s$ to $42p$ transition, which is detected by selective field ionization of the $42p$ atoms during the field ionization pulse. As shown, the $42p$ signal is earlier than the $42s$ signal. The shift and broadening of the microwave transition are used to determine the fields in the plasma.

a $42s$ population which only fluctuates by 5% from shot to shot [20]. The frequency fluctuations of a dye laser would lead to fluctuations of roughly a factor of 5 in the $42s$ population, but for excitation above the limit the frequency fluctuations are of no consequence. The atoms are then exposed to a 200 ns long microwave pulse to drive them to the $42p_{1/2}$ state. The microwaves are propagated through a glass window from a horn outside the vacuum system. Subsequent to the microwave pulse, a field-ionization pulse is applied to selectively detect the atoms which have made the transition to the $42p_{1/2}$ state. The field pulse also pushes ions or electrons of the plasma to the microchannel plate (MCP) detector. The microwave frequency is slowly swept through the $42s$-$42p$ resonance frequency over many shots of the pulsed lasers. The resonance line shapes are recorded as a function of the density of the plasma, the electron temperature of the plasma, and the time delay t after the initial formation of the plasma. The microwave power is reduced to the point that the observed resonances are 5 MHz wide, a limit determined by both the microwave pulse duration and the inhomogeneous magnetic trapping field. The density of the $42s$ atoms is kept low enough that there is no dipole-dipole broadening of the transition.

The field-ionization pulse can have either polarity. If it is positive it field ionizes the atoms and forces ions resulting from field ionization and all those created by the first laser pulse to the MCP detector. Since the pulse rises in 1μs the signals due to plasma ions, $42p$ atoms, and $42s$ atoms are resolved in time. If the polarity is negative, the electrons resulting from field ionization and those electrons trapped in the plasma are driven to the detector. Again, the signals are resolved in time. The initial geometry of the plasma and the atom samples are determined by the radius of the MOT, $r_m = 0.45$ mm, and the waists of the superimposed pulsed laser beams, both $r_w = 160$ μm.

We determine the number of ions we produce with each laser pulse by measuring the reduction in the number of atoms in the trap by the photoionization laser, a procedure similar to that employed by Singer *et al.* [21] and Han [22]. First, we measure $N_{\max}$, the maximum number of trapped atoms by measuring the fluorescence power from the MOT into a solid angle of 1.86×10^{-3} sr without the photoioization laser. Second, we measure the filling time of the MOT by observing the time-dependent fluorescence after the trapping lasers are turned on, yielding the filling time $\tau_{\text{fill}} = 0.85$ s. Finally, we measure N_{avg}, the time average number of atoms in the MOT when the photoionization pulses are present. The number of ions produced by each laser shot is given by

$$N_{\text{ion}} = (N_{\max} - N_{\text{avg}}) R \tau_{\text{fill}}, \tag{1}$$

where R is the repetition rate of the pulsed laser, 15 Hz. By observing the electron and ion signals with the field-ionization pulse applied with zero delay we determined the ratio of quantum efficiencies for electrons and ions to be 1.6(5).

The density of ions is a function of radial position in the trap perpendicular to the direction of the 480 nm beam propagation $r = \sqrt{x^2 + y^2}$, and the position in the propagation direction z. Explicitly, it is given by

$$\rho_I(r,z) = \rho_{I0} e^{-(r^2/r_w^2 + z^2/r_m^2)}, \tag{2}$$

where ρ_0 is the ion density at the center of the MOT. The relation between the total number of ions in the trap and the density at the center of the trap is obtained by integrating the density over the trap volume

$$N_i = \left(\frac{\sqrt{\pi}}{2}\right) \rho_{I0} r_w^2 r_m, \tag{3}$$

which is typically 4×10^4 ions.

III. OBSERVATIONS

We first measured the Stark shift of the $42s_{1/2}$-$42p_{1/2}$ transition in the presence of a static field. The shift arises from the difference in the polarizabilities of the two states, and it is characterized by $\Delta\nu = -\beta E^2$, where β is half the difference between the $42p_{1/2}$ and $42s_{1/2}$ polarizabilities, and E is the static field. These measurements yield $\beta = 33.0(3)$ MHz/(V/cm)^2.

Typical resonances in the presence of a plasma are shown in Fig. 3, for which the first laser was tuned 1 cm^{-1} above the ionization limit so as to make a nearly neutral plasma, and the second laser pulse was delayed from the first by 10 ns (i.e., in Fig. 2 $t = 10$ ns) to allow equilibration of the electrons but no motion of the ions. As the number of ions is increased from 0 to 2.4×10^4, the resonance shifts to lower frequency, with a maximum shift of 1.07(8) MHz, corresponding to a field of 0.6 V/cm. When the shifts of Fig. 3 are fit to an ion density

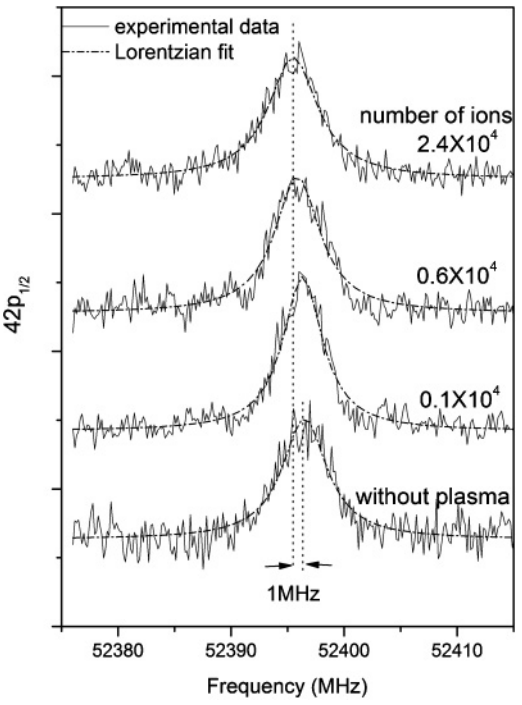

FIG. 3. $42s_{1/2}$ to $42p_{1/2}$ resonances in a nearly neutral plasma. The dash-dotted lines represent Lorentzian fits of the experimental data. The laser producing the plasma is tuned 1 cm^{-1} above the ionization limit to produce a nearly neutral plasma and the number of ion in the plasma is varied by adjusting the intensity of the laser. As more ions are produced, the resonant peak shifts further to the low frequency side due to the increasing microscopic field.

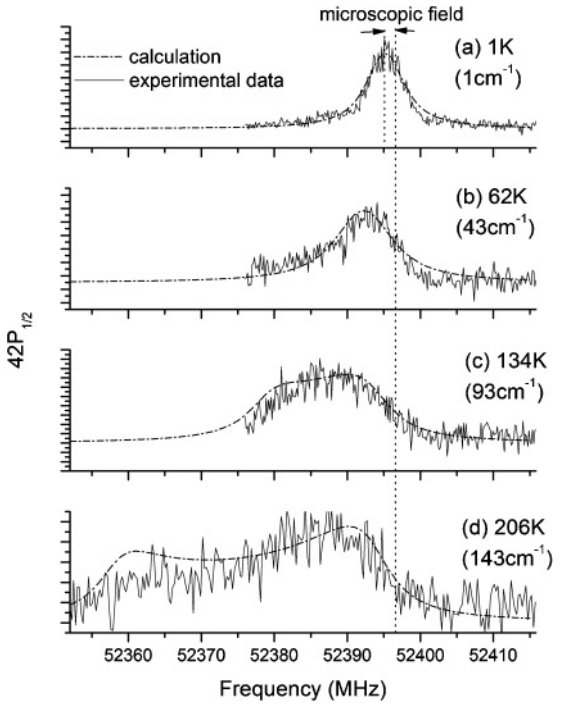

FIG. 4. $42s_{1/2}$ to $42p_{1/2}$ resonances in the presence of plasmas with different electron temperatures. In all cases the number of ions is 4×10^4. The dash-dotted lines represent the lineshape model. In (a) $T_e = 1$ K, there is only a microscopic field. For all higher temperatures, the microscopic field exists as background for the macroscopic field produced by the excess ions. As the laser frequency is tuned further above the ionization limit, the resonant peak tends to shift further to the low-frequency side and shows a non-Lorentzian profile due to the increasing charge imbalance between the electrons and ions in the plasma.

dependence, they vary as $\rho_I^{0.64(22)}$, in good agreement with the expected $\rho_I^{2/3}$ dependence.

If the tuning of the laser creating the plasma is raised from 1 to 143 cm^{-1} above the limit, we observe the results shown in Fig. 4. In all cases the same number of photoions, 4×10^4, is produced with the first laser pulse, and the second laser pulse is 10 ns after the first. As the first laser is tuned further above the limit we observe larger shifts, due to the increasing charge imbalance between the plasma electrons and ions. The ratios of the number of electrons to the number of ions at temperatures of 1, 62, 134, and 206 K, are 99(5)%, 89(7)%, 81(8)%, and 73(10)%. Furthermore, the lineshape becomes double peaked, which we attribute to the differences in the spatial distributions of the probe atoms, the ions, and the electrons.

To extract the plasma fields from the measurements shown in Fig. 4 we have developed a model for the lineshape. As shown by Fig. 1, the volume of plasma and Rydberg atoms excited by the 480 nm laser is a cylinder of height much larger than its diameter (i.e., $r_m \gg r_w$). Accordingly, as an approximation we assume that the ions and atoms are in an infinitely long cylinder with Gaussian radial densities given by

$$\rho_I(r) = (\rho_{I0}/a) e^{-r^2/r_w^2}, \tag{4a}$$

and

$$\rho_a(r) = (\rho_{a0}/a) e^{-r^2/r_w^2}, \tag{4b}$$

where, for example, ρ_{I0}/a is the average density of our 1 mm long plasma at $r = 0$, and a is a geometrical factor, which is given by $a = 1.42$ in our case. The microscopic field is determined by the distance to the nearest ion. Explicitly, its magnitude is given by

$$|E_{\text{micro}}| = \frac{1}{R_{NN}^2}, \tag{5}$$

where R_{NN} is the distance to the nearest ion. Using $\frac{4\pi}{3} R_{NN}^3 = \rho_I(r)$ leads to

$$|E_{\text{micro}}| = \left[\frac{3\rho_I(r)}{4\pi}\right]^{2/3}. \tag{6}$$

The microscopic field depends only on the ion density of the plasma, not on the temperature. It is highest at the center of the plasma/atom volume, and its direction is random. To compute the macroscopic field requires that we know the spatial distributions of both the ions and the electrons. Once we know them, applying Gauss' law to the ion and electron distributions we obtain the macroscopic plasma field. Explicitly, E_{macro} is given by

$$|E_{\text{macro}}(r)| = \int_0^r [\rho_I(r') - \rho_e(r')] r'\, dr', \tag{7}$$

and is in the radial direction. Here $\rho_e(r)$ is the electron density.

The motion of the ions in 200 ns is assumed to be negligible, and they are assumed to form an electrostatic trap for the plasma electrons. If the electrons were at zero temperature, they would have a Gaussian distribution identical to that of the ions, truncated at the radius r_T at which all the electrons have been used [23,24]. From Eq. (7), it is apparent that such a distribution would result in zero macroscopic field at radial distances smaller than the truncation radius r_T and nonzero fields at larger radial distances. However, for $r < r_T$, there would still be a microscopic field due to the nearest-neighbor ions. The electrons are not at zero temperature, and we have found that assuming them to have a radial Gaussian distribution $\rho_e(r) = \rho_{e0} e^{-r^2/r_c^2}$ of adjustable width and a fixed number of electrons, equal to what we measure, provides a reasonably good representation of our data, as shown by the fits of Fig. 4.

We assume the resonance lineshape $L(\nu,r)$ for an atom at radial position r to be given by

$$L(\nu,r) = \frac{W^2}{4[\nu - \nu_0 + \beta E^2(r)]^2 + W^2}, \tag{8}$$

where W is the full width at half maximum of the resonance observed in the absence of a plasma, and the squared total field is given by

$$E^2(r) = E_{\text{micro}}^2(r) + E_{\text{macro}}^2(r). \tag{9}$$

For all the measurements $W = 5.2$ MHz. Averaging $L(\nu,r)$ over the volume occupied by the atoms gives the lineshape $L(\nu)$, which can be compared to our observations, as shown in Fig. 4. Explicitly,

$$L(\nu) = \frac{\int L(\nu,r)\rho_a(r)\, dr}{\int \rho_i(r)\, dr}, \tag{10}$$

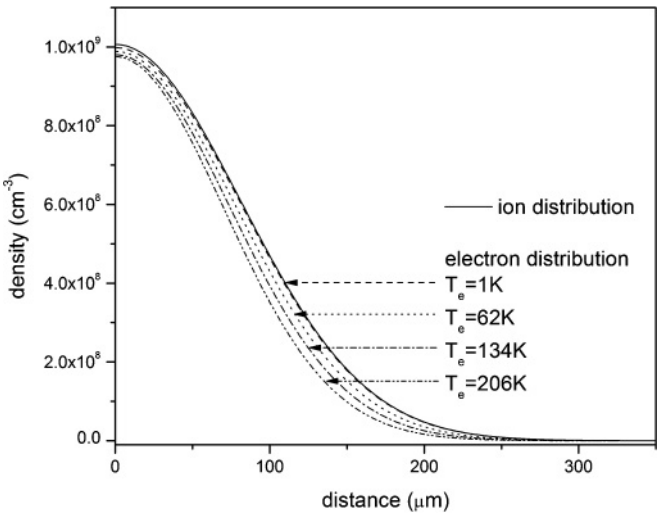

FIG. 5. Radial ion and electron distributions. The width of the electron cloud is determined by the best fit of the lineshape model in Fig. 2. As the laser is tuned further above the ionization limit, there are fewer electrons left in the plasma since more electrons escape from the ion cloud due to their higher kinetic energy.

where $\rho_a(r)$ is the density of $42s$ atoms, which is proportional to the ion density. The fits shown in Fig. 4 are obtained from the radial electron distributions $\rho_e(r)$ shown in Fig. 5. Also shown are the ion distributions (the atom distributions have the same form as the ion distributions.). As shown by Fig. 5, there are fewer electrons when the laser is tuned further above the limit since a greater charge imbalance is required to retain more energetic electrons. In Fig. 6 we show the microscopic and macroscopic fields in the plasma as well as the atom density weighted by r, to indicate which fields are being sampled by the atoms. The microscopic field is the same in all cases, and its maximum is at the center of the plasma, as shown. The macroscopic field is zero in the center of the plasma, increases to a maximum, and then decreases with radial position. Inspecting the fields of Fig. 6 we can see that at $T = 1$ K the microscopic field is dominant, but at all higher temperatures the macroscopic field is dominant, leading to larger shifts and the double-peaked lineshape observed at $T = 206$ K.

Delaying the second pulse allows us to observe the time evolution of the plasma. With the photoionization laser tuned 1 cm^{-1} above the limit we photoionize 4×10^4 atoms, and the number of electrons in the plasma decreases with time. When we observe the $42s$-$42p$ transition as a function of the delay of the second laser we observe the set of resonances shown in Fig. 7. With 10 ns of delay the resonance is shifted to 1 MHz below the atomic frequency due to the microscopic fields. The frequency shift increases as the delay t is increased until it reaches a maximum of 2.5 MHz at a delay of 4 μs, and with longer delays the shift decreases. A qualitative explanation of these observations is that for the first 4 μs after its creation the plasma loses a substantial number of electrons, developing a growing charge imbalance, which leads to an increasing macroscopic field and frequency shift of the $42s$-$42p$ resonance. After 4 μs the expansion of the plasma

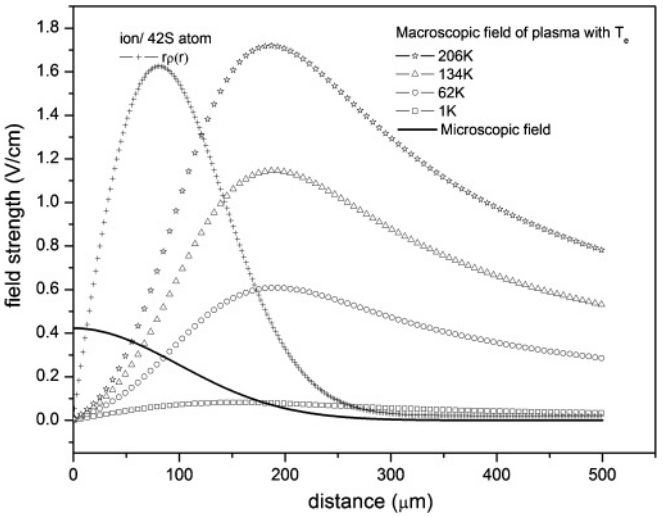

FIG. 6. The microscopic and macroscopic fields of plasmas with various temperatures. The microscopic field is dominant in the $T_e = 1$ K plasma since the plasma is nearly neutral. In the other plasmas, the macroscopic field is stronger than the microscopic field.

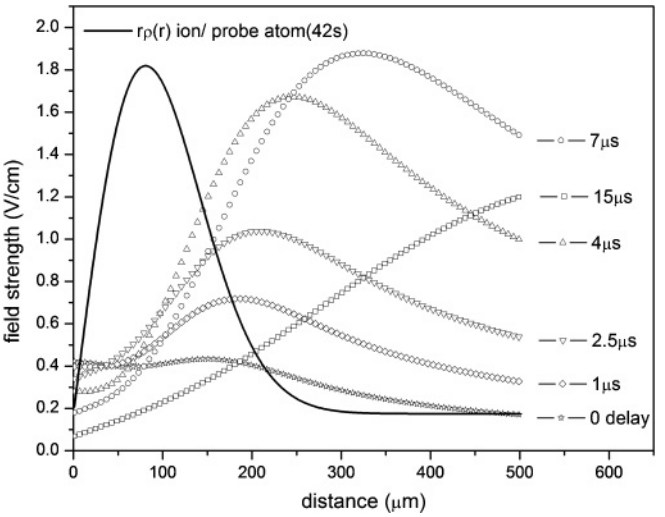

FIG. 8. The sum of the calculated microscopic and macroscopic fields for the best fits to the observed data in Fig. 5. The total field reaches its maximum in the central region where the probe atoms (42s atoms) are located at 4 μs. At later times the field at the location of the atoms decreases although the peak field, at larger radial distance, continues to increase.

lowers both the microscopic and macroscopic fields at the center of the plasma, where the probe atoms are located.

A more quantitative description along the lines above can be developed if we know the size of the ion cloud. We use the temporal broadening of the photoion signal with delay time to determine the size of the ion cloud. The correlation between the time when we detect an ion and its position before the field pulse is determined by translating the photoionization laser beam and observing the change in the time at which we detect the ions using a field pulse applied immediately after laser excitation.

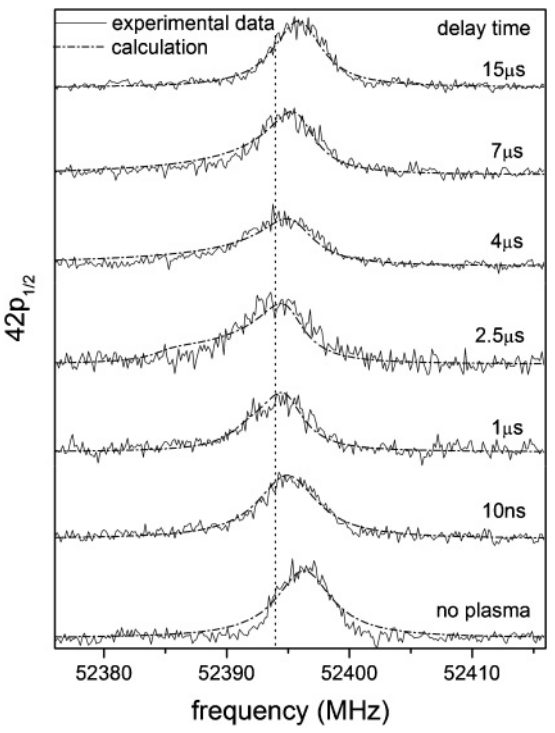

FIG. 7. $42s_{1/2}$ to $42p_{1/2}$ resonances as a function of delay time between the plasma laser and the probe laser. The dash-dotted lines represent the best fits of the lineshape model to the observed resonances. At early times, until 2.5 μs, the resonant peak shifts to lower frequency due to the creation of the excess ions. For delays in excess of 2.5 μs the peak shifts back to the atomic frequency due to the expansion of the ion cloud.

We assume that the ion cloud expands as a Gaussian with radius $r_{\rm exp}(t)$ given by [8]

$$r_{\rm exp}^2(t) = r_w^2 + (v_0 t)^2, \tag{11}$$

where v_0 is the initial velocity of the plasma. Choosing the initial velocity $v_0 = 40$ m/s provides an excellent fit to our observations, and this velocity is consistent with the observations of Kulin *et al.* [8]. Using the radius of the ion cloud from Eq. (11) and the procedure used to fit the zero delay data of Fig. 4 we fit the observed lineshapes of Fig. 7. For each delay time we know the number of ions and their spatial distribution, as well as the number of electrons. The electrons are again assumed to have a Gaussian distribution which is adjusted to produce the fit curves of Fig. 7, which reproduce the experimental curves reasonably well. The combined electron and ion distributions lead to the total field distributions shown in Fig. 8. For delay times longer than 4 μs the plasma has expanded so much that the macroscopic field is only large outside the Rydberg atom cloud, which does not expand but has the same diameter it had at zero delay.

IV. CONCLUSION

We have demonstrated a sensitive new method for measuring the fields in low-density plasmas, measuring the Stark shift of a microwave transition between Rydberg states. Using this technique we have been able to measure both the

macroscopic and microscopic fields in an ultracold plasma. In these measurements we have a sensitivity to fields as small as 0.1 V/cm. They can be improved and extended in several ways. Sensitivity to substantially smaller fields could be obtained by observing, for example, the Rb $40d$ to $39f$ transition, which has a larger Stark shift, and by turning off the inhomogeneous trap magnetic fields. In a plasma of 1 mm diameter it should be possible to make a spatially resolved field measurement by exciting small volumes of Rydberg atoms with crossed focused laser beams. Achieving a spatial resolution of 50 μm should be straightforward.

ACKNOWLEDGMENT

This work has been supported by the Air Force Office of Scientific Research.

[1] T. C. Killian, S. Kulin, S. D. Bergeson, L. A. Orozco, C. Orzel, and S. L. Rolston, Phys. Rev. Lett. **83**, 4776 (1999).
[2] T. Killian, T. Pattard, T. Pohl, and J. Rost, Phys. Rep. **449**, 77 (2007).
[3] S. L. Rolston, Physics **1**, 2 (2008).
[4] D. J. Wineland, J. C. Bergquist, W. M. Itano, J. J. Bollinger, and C. H. Manney, Phys. Rev. Lett. **59**, 2935 (1987).
[5] F. Diedrich, E. Peik, J. M. Chen, W. Quint, and H. Walther, Phys. Rev. Lett. **59**, 2931 (1987).
[6] M. S. Murillo, Phys. Rev. Lett. **87**, 115003 (2001).
[7] C. E. Simien, Y. C. Chen, P. Gupta, S. Laha, Y. N. Martinez, P. G. Mickelson, S. B. Nagel, and T. C. Killian, Phys. Rev. Lett. **92**, 143001 (2004).
[8] S. Kulin, T. C. Killian, S. D. Bergeson, and S. L. Rolston, Phys. Rev. Lett. **85**, 318 (2000).
[9] F. Robicheaux and J. D. Hanson, Phys. Rev. Lett. **88**, 055002 (2002).
[10] T. C. Killian, M. J. Lim, S. Kulin, R. Dumke, S. D. Bergeson, and S. L. Rolston, Phys. Rev. Lett. **86**, 3759 (2001).
[11] R. S. Fletcher, X. L. Zhang, and S. L. Rolston, Phys. Rev. Lett. **99**, 145001 (2007).
[12] T. Pohl, D. Vrinceanu, and H. R. Sadeghpour, Phys. Rev. Lett. **100**, 223201 (2008).
[13] V. L. Jacobs, J. Davis, and P. C. Kepple, Phys. Rev. Lett. **37**, 1390 (1976).
[14] Henry Margenau and William W. Watson, Rev. Mod. Phys. **8**, 22 (1936).
[15] H. R. Griem, *Plasma Spectroscopy* (McGraw-Hill, New York, 1964) pp. 72–78.
[16] B. N. Ganguly and A. Garscadden, Appl. Phys. Lett. **46**, 540 (1985).
[17] D. K. Doughty and J. E. Lawler, Appl. Phys. Lett. **45**, 611 (1984).
[18] D. Feldbaum, N. V. Morrow, S. K. Dutta, and G. Raithel, Phys. Rev. Lett. **89**, 173004 (2002).
[19] W. Li, P. J. Tanner, Y. Jamil, and T. F. Gallagher, Eur. Phys. J. D **40**, 27 (2006).
[20] M. P. Robinson, B. Laburthe Tolra, M. W. Noel, T. F. Gallagher, and P. Pillet, Phys. Rev. Lett. **85**, 4466 (2000).
[21] K. Singer, M. Reetz-Lamour, T. Amthor, L. G. Marcassa, and M. Weidemuller, Phys. Rev. Lett. **93**, 163001 (2004).
[22] J. Han, Ph.D. thesis, University of Virginia, 2009.
[23] D. J. Wineland, J. J. Bollinger, W. M. Itano, and J. D. Prestage, J. Opt. Soc. Am. B **2**, 1721 (1985).
[24] R. D. Knight and M. H. Prior, J. Appl. Phys. **50**, 3044 (1979).